JOURNAL OF GEOPHYSICAL RESEARCH, VOL. 112, C06007, doi:10.1029/2006JC003568, 2007

Click Here for Full Article

# Does eddy subduction matter in the northeast Atlantic Ocean?

Geoffrey Gebbie[1,2]

Received 1 March 2006; revised 1 February 2007; accepted 22 February 2007; published 12 June 2007.

[1] Mesoscale eddies are an important contributor to subduction in the Gulf Stream region and the Antarctic Circumpolar Current, but is eddy subduction also important in the relatively quiescent interior of the world's subtropical gyres? Observations from the Subduction Experiment of the northeast Atlantic do not have the spatial resolution necessary to calculate eddy subduction and answer this question. Regional numerical models can diagnose subduction, but their representativeness is unknown. Furthermore, water mass budgets in an open-ocean domain show that the simulated properties of subducted water directly depend upon uncertain open-boundary conditions and surface fluxes. To remedy these problems, a state estimate of the ocean circulation is formed by constraining an eddy-permitting general circulation model to observations by adjusting the model parameters within their uncertainty. The resulting estimate is self-consistent with the equations of motion and has the necessary resolution for diagnosing subduction. In the northeast Atlantic during 1991–1993, the time-variable circulation contributes less than 1 Sv of net subduction, while the total subduction is 4 Sv. Eddy volume fluxes of 40 m/yr in the North Equatorial Current and the Azores Current, however, are significant and rival the subduction by Ekman pumping locally. Furthermore, a state estimate at 1/6° resolution has 2–3 Sv more subduction in the density bands centered around $\sigma$ = 24.0 kg/m$^3$ and $\sigma$ = 26.0 kg/m$^3$ than a 2° state estimate. This result implies that the inability to accurately simulate mesoscale phenomena and surface fluxes in climate models would lead to an accumulation of errors in water mass properties over 10–20 years, even in the interior of the subtropical gyre.

**Citation:** Gebbie, G. (2007), Does eddy subduction matter in the northeast Atlantic Ocean?, *J. Geophys. Res.*, *112*, C06007, doi:10.1029/2006JC003568.

## 1. Introduction

[2] Ekman convergence occurs throughout the subtropical gyre, generally forcing surface waters downward into the main thermocline. The permanent transfer of fluid from the mixed layer to the deeper ocean is called "subduction" [*Cushman-Roisin*, 1987]. By the process of subduction, surface water modifications lead to changes in the structure of the interior ocean at middepths. The subduction regions of the ocean are grossly related to the large-scale wind forcing by Ekman convergence, but the deviations from this zero-order picture are significant. Rates of Ekman pumping, typically 30 m/yr, are usually much smaller than the subduction rates observed by tracer studies, such as the 80 m/yr inferred by Helium-Tritium tracer studies [*Jenkins*, 1987]. These differences can be partially explained by horizontal currents which subduct water across a sloping mixed-layer base, called "lateral induction" [*Woods*, 1985; *Cushman-Roisin*, 1987; *Marshall et al.*, 1993]. Smaller-scale features of the circulation, such as semipermanent fronts, also complicate the story. In the Azores Current, the characteristics of subducted water depend upon the depth in which they intersect the front [*Robbins et al.*, 2000], which suggests that frontal dynamics may be important. On the basis of these previous studies, both the amounts of subduction and the physical processes which produce subduction are uncertain.

[3] One potentially significant small-scale process is subduction by the mesoscale eddy field, so-called "eddy subduction." *Follows and Marshall* [1994] estimated that eddy fluxes across typical oceanic fronts drive subduction with a magnitude comparable to the mean flow. For example, in the Antarctic Circumpolar Current (ACC), the subduction of Antarctic Intermediate Water is not adequately captured by mean subduction rates [*Marshall*, 1997], and only by considering the impact of eddies can the interior ocean structure be explained. In the Gulf Stream region, subduction in one numerical model has been shown to be dominated by eddy-scale motions with rates up to 150 m/yr [*Hazeleger and Drijfhout*, 2000]. Whenever investigators have looked at "eddy-rich" regions, eddy subduction is important, but could eddies play a large role even in the relatively quiescent regions of the ocean?

[4] To assess the relative importance of eddy subduction, we have chosen a region with a large supply of observa-

[1]Massachusetts Institute of Technology/Woods Hole Oceanographic Institution Joint Program in Oceanography, Woods Hole, Massachusetts, USA.

[2]Now at Department of Earth and Planetary Sciences, Harvard University, Cambridge, Massachusetts, USA.


0148-0227/07/2006JC003568$09.00

tions. The eastern subtropical gyre of the North Atlantic Ocean (hereafter, northeast Atlantic) was host to the Subduction Experiment, a large-scale observational campaign from 1991 to 1993 [*Brink et al.*, 1995]. Direct calculation of subduction rates is not possible with the Subduction Experiment observations owing to a lack of spatial resolution. Numerical models are a natural way to solve the resolution problem; for example, *Spall et al.* [2000] used a model which compared well with observations in order to diagnose subduction. An extension of the methodology of *Walin* [1982] to an open-ocean domain, however, shows that the properties of subducted water depend upon open-boundary velocities and air-sea fluxes: two quantities which are highly uncertain in any regional model simulation (section 2). A "state estimate" is the statistical combination of a model and observations subject to their relative uncertainties. Such an estimate of the circulation is introduced in section 3 to account for the shortcomings inherent in analysis of models or observations alone. A companion paper [*Gebbie et al.*, 2006] dealt with the methodology of creating such an estimate and only an overview is presented here. The state estimate has the prerequisite spatial and temporal resolution to directly calculate subduction rates (section 4.1) and the contribution by mesoscale eddies, the focus of this work (sections 4.2 and 4.3). As will be seen, small-scale intense regions of subduction are located near fronts and strong currents. Although some data assimilation products introduce artificial sources and sinks, this state estimate is self-consistent with the equations of motion, and hence, the properties of subducted water can be attributed to physical processes (section 4.4). Section 5 summarizes the results, and discusses the implications of this finding on decadal climate model integrations.

## 2. Subduction and Transformation in an Open-Ocean Domain

[5] A complete understanding of subduction must explain how subducted water gets its properties and how subducted water gets forced downward. These questions require the tracking of water masses in the oceanic mixed layer. Following the inspiration of previous investigators [*Walin*, 1982; *Tziperman*, 1986; *Speer and Tziperman*, 1992], potential density is used to classify water masses. (Specifically, we use $\sigma_\theta$ for potential density, and because $\sigma_\theta = \sigma_t$ in the surface layer, we drop the subscript.) These previous works were applied to entire ocean basins, and an extension of these methods has been developed independently by *Large and Nurser* [2001], *Gebbie* [2004], and *Donners et al.* [2005] for an open-ocean region of interest. This section reviews the definition of subduction and how subduction fits into open-ocean isopycnal budgets, with emphasis on the role of the mesoscale eddy field.

### 2.1. Kinematic Definition of Subduction

[6] If $h(x, y)$ is the depth of the mixed layer, then the volume flux across $h$ per unit area is called the "local subduction rate":

$$s(x,y,t) = -\frac{\partial h}{\partial t} - w_h - \mathbf{u}_h \cdot \nabla h, \tag{1}$$

where $w_h$ is the vertical velocity at $h$ and $\mathbf{u}_h$ is the two-component horizontal velocity at $h$ [*Cushman-Roisin*, 1987]. To find the net subduction in a particular density band, first denote $\mathcal{A}_h(\sigma, t)$ to be the surface defined by the base of the mixed layer with density less than $\sigma$. Then the net subduction at densities less than $\sigma$ is obtained by integrating (1) over $\mathcal{A}_h(\sigma, t)$:

$$S_h(\sigma,t) \equiv \int^{\mathcal{A}_h(\sigma,t)} \left(-\vec{\mathbf{v}}_h \cdot \hat{\mathbf{n}}_h\right) d\mathcal{A} = \int^{\mathcal{A}_h(\sigma,t)} s(x,y,t)\, d\mathcal{A}, \tag{2}$$

where $\vec{\mathbf{v}}_h$ is the three-dimensional velocity relative to the moving reference frame of $\mathcal{A}_h$, and $\hat{\mathbf{n}}_h$ is the direction normal to $\mathcal{A}_h$. (The reason for the subscript "h" on S will become clear shortly.) Equation (2) is the kinematic or direct method to compute water mass subduction rates. The net subduction in a density band $\sigma_1 < \sigma < \sigma_2$ is simply $S_h(\sigma_2, t) - S_h(\sigma_1, t)$.

[7] Both the area of subduction, $\mathcal{A}_h(\sigma, t)$, and the normal velocity across the surface, $\vec{\mathbf{v}}_h\, \hat{\mathbf{n}}_h$, vary with time. Following *Marshall* [1997] and the derivation in Appendix A, the time-mean water mass subduction rate can be decomposed into three parts:

$$\overline{S_h}(\sigma) = \int^{\overline{\mathcal{A}_h}(\sigma)} -\left(\overline{w}_h + \overline{\mathbf{u}}_h \cdot \nabla \overline{h}\right) d\mathcal{A} + \int^{\overline{\mathcal{A}_h}(\sigma)} -\overline{\left(\frac{\partial h'}{\partial t} + \mathbf{u}'_h \cdot \nabla h'\right)} d\mathcal{A} + \overline{\int^{\mathcal{A}'_h(\sigma,t)} s(x,y,t)\, d\mathcal{A}}, \tag{3}$$

where the overbar indicates a time mean and the primed quantities are temporal anomalies. $\overline{\mathcal{A}_h}(\sigma)$ is the surface area defined by the position of the mean isopycnals at the mean mixed-layer depth, and the integral over $\mathcal{A}'_h(\sigma, t)$ is a mathematical shorthand for the impact of the time-varying isopycnals (defined fully in Appendix A). The eddy subduction rate is defined as the second and third integrals of the right-hand side of (3). The third integral of (3) is slightly different than what *Marshall* [1997] derived; a more complete discussion of this point is included in Appendix A.

[8] *Marshall* [1997] did not explicitly deal with the seasonal cycle when decomposing the mean and eddy components of subduction. A majority of the water that leaves the mixed layer is later reentrained by the vertical excursions of the mixed-layer base [*Stommel*, 1979; *Marshall et al.*, 1993; *Williams et al.*, 1995]. Also, variations due to the seasonal cycle will dominate the eddy subduction terms if a simple time-mean or running average is taken. In the case where the seasonal cycle of velocity and density is well known, then the primed quantities in (3) can be redefined relative to the seasonal mean, but this is not the case generally. Next, we show one method to address this issue.

[9] To better isolate the waters that are permanently subducted, the bottom boundary can be fixed at the maximum mixed-layer depth over the year where the fixed boundary is denoted $H(x, y) = \max(h[x, y, t])$ [e.g., *Marshall*

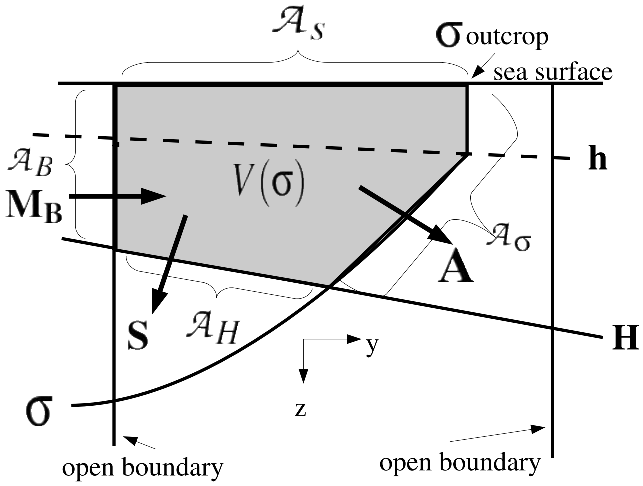


**Figure 1.** A meridional-depth section of the surface-layer control volume at density less than $\sigma$ (shaded). The volume of the surface layer with density less than $\sigma$ is $V(\sigma, t)$, and is bounded by an isopycnal, the maximum mixed-layer depth at depth $H(x, y, t)$, the sea surface, and the regional boundary. These surfaces have areas $\mathcal{A}_\sigma(\sigma, t)$, $\mathcal{A}_H(\sigma, t)$, $\mathcal{A}_s(\sigma, t)$, and $\mathcal{A}_B(\sigma, t)$. The control volume can also be defined with the bottom boundary as the time-variable mixed-layer depth, $h(t)$, with area $\mathcal{A}_h(\sigma, t)$. For the volume budget, the thick arrows represent volume fluxes through the faces of the control volume: $M_B(\sigma, t)$ for the boundary flux, $A(\sigma, t)$ for diapycnal flux, and $S(\sigma, t)$ for the flux across the mixed-layer base, the water mass subduction rate.

*and Nurser*, 1991; *Marshall et al.*, 1999]. Equation (3) can be rewritten with the fixed lower boundary:

$$\overline{S_H}(\sigma) = \int^{\overline{\mathcal{A}_H}(\sigma)} -(\overline{w}_H + \overline{\mathbf{u}}_H \cdot \nabla H)\, d\mathcal{A} + \overline{\int^{\mathcal{A}'_H(\sigma,t)} -\ (w_H + u_H \cdot \nabla H)\, d\mathcal{A}}, \tag{4}$$

where the water mass subduction rate now has a subscript "*H*" and the second integral of the right-hand side is the corresponding eddy subduction rate. Note that $H$ is constant in time, and therefore this definition of eddy subduction is simpler than the previous one. The direct impact of the seasonal cycle is eliminated in equation (4), but this expression should be viewed as an imperfect approximation to the water mass subduction rate.

### 2.2. Thermodynamic Method to Compute Subduction

[10] Regardless of which bottom boundary is chosen, subduction is only one part of the surface-layer volume budget. Isopycnal budgets were traditionally derived in the context of an infinitesimal layer of density $\sigma$ to $\sigma + \delta\sigma$. Here the isopycnal budgeting will be applied to a general circulation model (GCM), so isopycnal budgets are derived within discrete density bands: more specifically, all densities between 0 and an arbitrary $\sigma$. With discrete density bands, we prefer the name "water mass" budget instead of isopycnal budget. In our formulation, the oceanic mixed layer is bounded by four surfaces, $\mathcal{A}_h$, $\mathcal{A}_\sigma$, $\mathcal{A}_B$, and $\mathcal{A}_s$: the base of the mixed layer, an isopycnal, the domain boundary, and the sea surface, respectively. With the choice of $H(x, y)$ as the bottom boundary, the control volume is bounded by the surface $\mathcal{A}_H$ on the bottom and is more correctly called the "surface layer" rather than the mixed layer (see Figure 1).

[11] The control volume, $V(\sigma, t)$, at density less than an arbitrary potential density, $\sigma$, is affected by volume sources and sinks:

$$\frac{\partial V(\sigma,t)}{\partial t} = M_B(\sigma,t) - A(\sigma,t) - S(\sigma,t), \tag{5}$$

where $M_B(\sigma, t)$ is the volume flux through the open boundaries in the same density range, $A(\sigma, t)$ is the advective diapycnal volume flux, and $S(\sigma, t)$ can be subduction across either the time-variable or fixed bottom boundary. Volume flux through the surface by evaporation, precipitation, and runoff is much smaller than the other fluxes and may be neglected.

[12] The flow across isopycnals, $A(\sigma, t)$ in equation (5), implies a transformation of water into a new density class. For transformation to occur, there must be a convergence of buoyancy flux in a density band. In particular, $A(\sigma, t)$, the advective flux of buoyancy across the isopycnal $\sigma$, must be balanced by (1) the convergence of atmospheric buoyancy forcing, $F_S(\sigma, t)$, (2) diffusive flux convergence across isopycnals and the mixed-layer base, $F_D(\sigma, t)$, and (3) a new term, $F_B(\sigma, t)$, for open-ocean boundary effects. The density of an isopycnal is fixed by definition, and thus the diapycnal advection of fluid is exactly balanced by transformation:

$$A(\sigma,t) = F_S(\sigma,t) + F_D(\sigma,t) + F_B(\sigma,t). \tag{6}$$

[13] The first two terms of the right-hand side, $F_S(\sigma, t)$, and $F_D(\sigma, t)$, are detailed in previous works [e.g., *Walin*, 1982; *Tziperman*, 1986; *Garrett et al.*, 1995; *Nakamura*, 1995; *Garrett and Tandon*, 1997; *Marshall et al.*, 1999]. The term $F_B(\sigma, t)$ is water mass transformation due to the open boundary ($F_{edge}$ in the work of *Large and Nurser* [2001]). $F_B(\sigma, t)$ is calculated in a similar way as $F_D(\sigma, t)$. Following *Marshall et al.* [1999] but changing the boundary, we obtain

$$F_B(\sigma,t) = -\frac{\partial}{\partial\sigma}\int^{\mathcal{A}_B}\left(\mathbf{N}\cdot\hat{\mathbf{n}}_B\right)d\mathcal{A}, \tag{7}$$

where $\mathbf{N}$ is the diffusive buoyancy flux and $\mathbf{N}\ \hat{\mathbf{n}}_B$ is the flux directed across $\mathcal{A}_B$.

[14] The properties of subducted fluid, $S(\sigma, t)$, are set by the combined constraints of volume and buoyancy conservation. Combining equations (5) and (6) gives

$$S(\sigma,t) = -\frac{\partial V(\sigma,t)}{\partial t} + M_B(\sigma,t) - F_S(\sigma,t) - F_D(\sigma,t) - F_B(\sigma,t), \tag{8}$$

which is called the indirect or thermodynamic method for computing subduction rates.

[15] As implied by equation (8), an accurate model simulation of the properties of subducted water must represent a number of processes. Subduction, therefore, will

depend upon model inputs, such as open-boundary fields in $M_B(\sigma, t)$ and surface forcing fields in $F_S(\sigma, t)$, as well as the internal ocean physics implicit in the terms $F_D(\sigma, t)$ and $F_B(\sigma, t)$.

[16] Thermodynamic estimates of eddy subduction are possible, as the terms $\overline{M_B(\sigma)}$ and $\overline{F_S(\sigma)}$, for example, can involve eddy correlations. Together with section 2.1, we have now shown three methods for computing eddy subduction rates.

## 3. A State Estimate of the Northeast Atlantic

[17] The northeast Atlantic Ocean is an ideal location to compute subduction rates because of the intensive field campaign of the Subduction Experiment [*Brink et al.*, 1995]. Even with the Subduction Experiment meteorological mooring data, open-ocean information about atmospheric properties is notoriously biased and uncertain. Section 2.2 showed that the properties of subducted water depend greatly on these quantities. A promising approach is to form a statistical combination of observations and model, a "state estimate." Such an estimate is advantageous because it uses many different forms of information, it has improved and evenly spaced resolution, and it is self-consistent with the equations of motion such that dynamical balances can be naturally interpreted.

### 3.1. Method of State Estimation

[18] A companion paper [*Gebbie et al.*, 2006] detailed the methodology of estimating the circulation of the northeast Atlantic Ocean. The goal was estimation of the time-varying circulation during part of the Subduction Experiment, specifically June 1992 to June 1993. The state estimate is consistent with many data sets, such as the subsurface mooring measurements of the Subduction Experiment, and it includes the TOPEX/POSEIDON satellite altimetry data which have not previously been compared to the in situ data. The circulation of the northeast Atlantic region is also consistent with the ECCO (Estimating the Climate and Circulation of the Ocean) Consortium global 2° state estimate [*Stammer et al.*, 2002] and the dynamics of the MIT General Circulation Model (MITgcm) [*Marshall et al.*, 1997] including the KPP boundary layer scheme [*Large et al.*, 1994]. The resulting state estimate has 23 vertical levels, 1/6° horizontal resolution ($\approx$15 km) resolution, and a twin estimate at 2° horizontal resolution.

[19] To form the state estimate, a regional eddy-permitting GCM was nested within the ECCO coarse-resolution global state estimate (hereafter, "ECCO Global Estimate"). In other words, first-guess initial conditions and open-boundary conditions were taken from the ECCO product and applied to the regional model. The MITgcm was implemented with Dirichlet boundary conditions, and the boundary fields were prescribed without any radiation scheme. A sponge layer was introduced to damp any spurious waves. A cost function, defined as the misfit between observations and model, was then evaluated. The first-guess model simulation did not predict the observations within their uncertainty, so an adjoint model [*Marotzke et al.*, 1999] was then used to adjust the uncertain model parameters and forcings (initial conditions, surface forcings, open-boundary conditions) in a iterative way until the modeled trajectory was consistent with the observations (the "adjoint method") [e.g., *LeDimet and Talagrand*, 1986; *Tziperman and Thacker*, 1989]. A posterior check showed that the parameters were adjusted within reasonable bounds.

### 3.2. Hydrography and Circulation of the Northeast Atlantic: 1991–1993

[20] The use of observations is critical to the upper ocean hydrographic structure in the model, in particular, the mixed-layer depth (MLD). Because subduction by lateral induction depends upon horizontal gradients of MLD, errors in the upper ocean hydrography must be minimized. The first-guess model simulation (unconstrained by observations) is too warm in the Azores Current (AC) region and too cold at 24°N. A consequence is wintertime MLDs which are too shallow at the Northwest mooring site, and too deep to the west of the Central mooring (Figure 2). When the northeast Atlantic model is constrained by observations (the state estimate, Figure 3), the mooring MLDs are generally reproduced within 20 m, as opposed to the 60 m errors in the unconstrained model. State-estimate MLD shoals equatorward of 25°N, in accordance with climatologies [*Marshall et al.*, 1993; *Levitus and Boyer*, 1994]. The region between 25°N and 35°N, however, hardly has an equatorward gradient of mixed-layer depth, which is surprising, but in accordance with the observational synthesis of *Weller et al.* [2004].

[21] The mean circulation of the upper ocean is dominated by the Azores Current with speeds up to 20 cm/s (Figure 4). The AC volume transport is about 12 Sv at 40°W, diminishing to roughly 3 Sv near the Mediterranean outflow. The estimated AC has similar width and transport as found in surveys by research vessels [*Rudnick and Luyten*, 1996; *Joyce et al.*, 1998]. Many North Atlantic models tend to have an erroneously weak AC, as discussed by *Jia* [2000] and *New et al.* [2001]. The east-west axis is at 36°N, farther north than the climatological position by 1–3° of latitude, but consistent with the recent synthesis of *Weller et al.* [2004] for the years 1991–1993.

### 3.3. State Estimate Diagnostics

[22] The state estimate is available on the same grid as the numerical model used here, the MITgcm. This GCM is a z-coordinate model and uses a C-Grid for the state variables. Transforming the z-coordinate model into isopycnal coordinates was discussed by *Marshall et al.* [1999], and we follow their approach. The mean location of the isopycnals at the depth of the maximum mixed layer is shown for reference in Figure 4. The GCM diagnostic routines are discussed in Appendix B and all calculations use 10-day average fields and density bins of 0.2 kg/m$^3$ unless otherwise noted.

## 4. Estimates of Northeast Atlantic Subduction

### 4.1. Kinematic Estimates of Subduction

[23] Following equation (2), subduction is directly calculated by the kinematic method from the 1/6° state estimate, then averaged over one year. Here subduction rates are calculated across the fixed maximum depth of the mixed layer ($\overline{S_H}(\sigma, t)$, Figure 5, top) and across the time-variable mixed-layer base ($\overline{S_h}(\sigma, t)$). A domain-integrated 4 Sv of

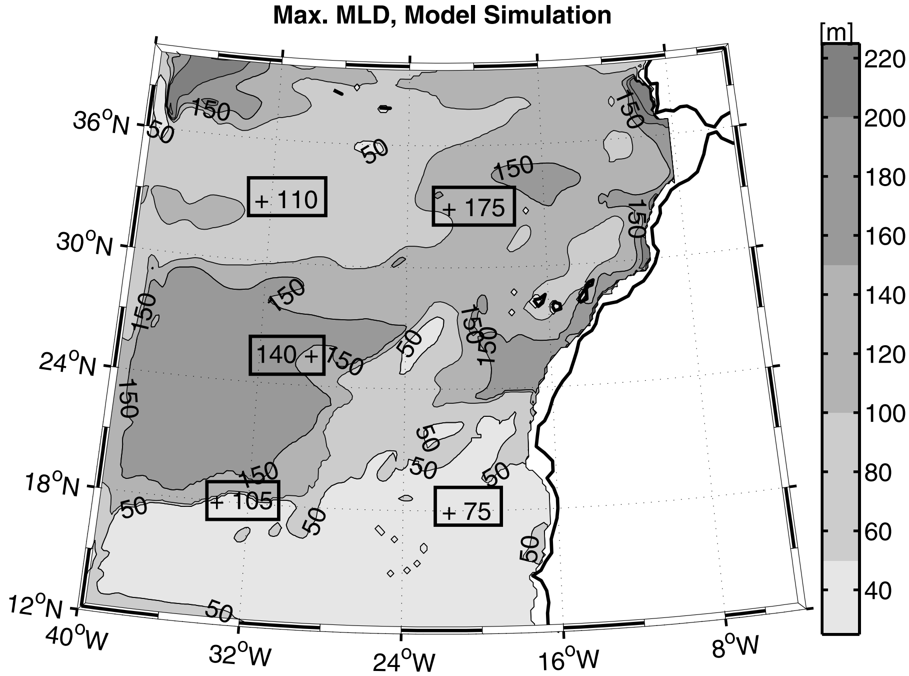


**Figure 2.** Shading denotes maximum mixed-layer depth for winter 1992–1993 in the unconstrained model simulation. The mixed layer is defined as the region where the density difference to the surface is less than 0.025 kg/m$^3$. Boxes denote maximum mixed-layer depth for the five Subduction Experiment moorings at locations marked by pluses. The full state estimate domain is plotted.

subduction is estimated with either choice of bottom boundary. Subduction across the time-variable mixed-layer base, however, systematically occurs at lower densities. The seasonal cycle of subduction rates (not pictured) shows that the "mixed-layer demon" of *Stommel* [1979] is active, and therefore $\overline{S_h}(\sigma, t)$ includes subducted water which will later be reentrained into the mixed layer. Lower density waters are preferentially reentrained and thus account for the primary differences between the two estimates. Another difference is the influx of waters through the changed lateral

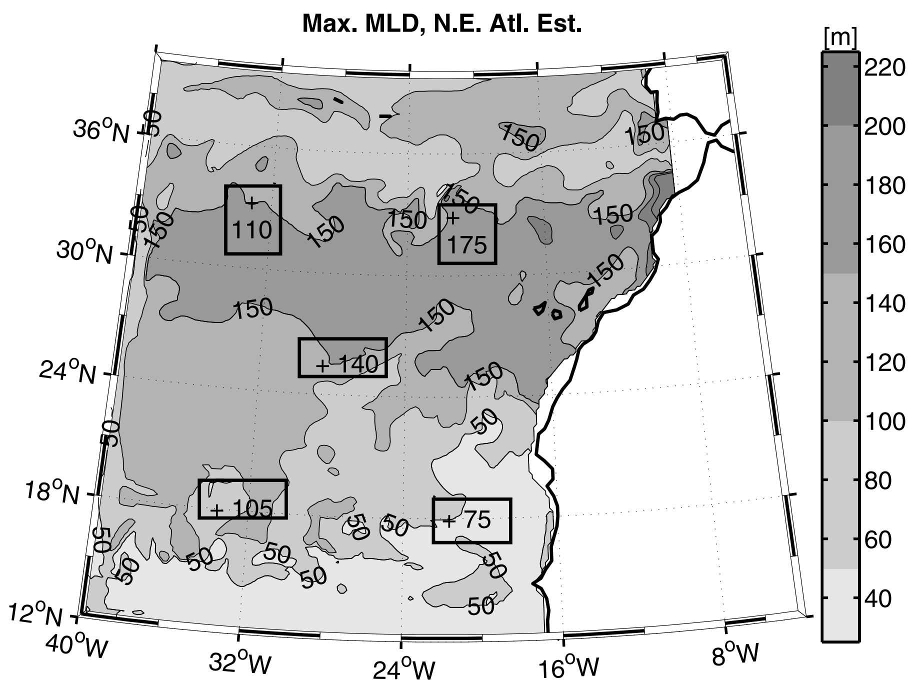


**Figure 3.** Shading denotes maximum mixed-layer depth for winter 1992–93 in the northeast Atlantic state estimate (constrained model). Boxes denote maximum mixed-layer depth at the Subduction Experiment moorings.

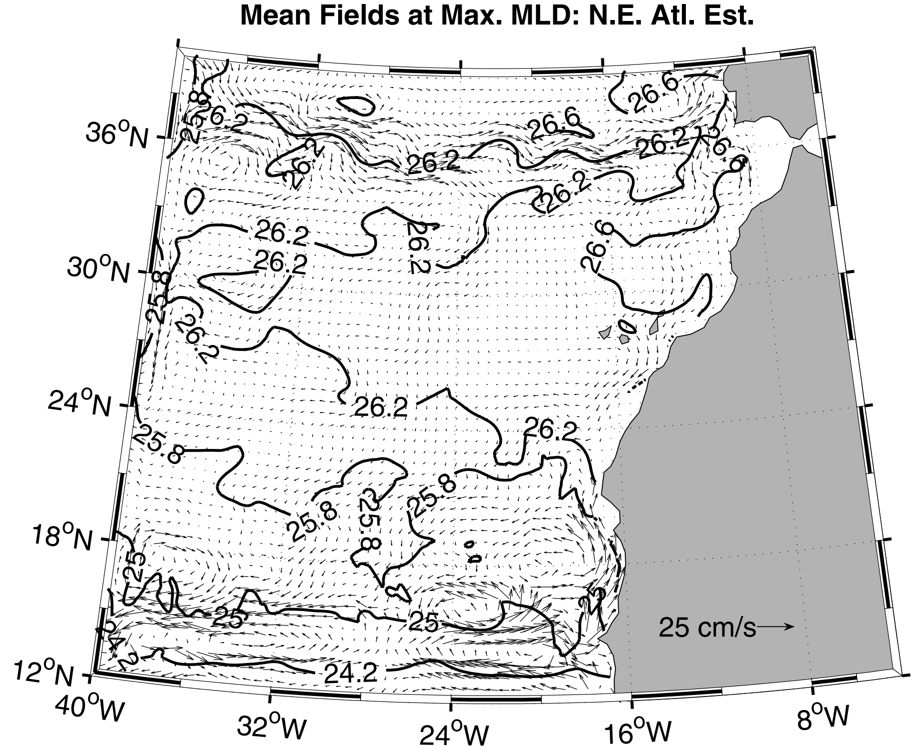


**Figure 4.** Annual-mean potential density and velocity field at the maximum mixed-layer depth for June 1992 to June 1993.

boundaries (to be discussed in section 4.4). Thus the choice of bottom boundary does affect the structure of the water mass subduction rates, in accord with *Valdivieso Da Costa et al.* [2005].

[24] To test whether lateral induction may be significant, the annual-mean subduction rate ($\overline{S_H}(\sigma)$) is split into vertical and horizontal components (Figure 5, middle). A domain-integrated 2 Sv of subduction is contributed by lateral induction (marked "horiz"), nearly equivalent to the subduction by vertical velocity.

[25] It is interesting to see how well the full subduction rate can be captured by substitution of the annual-average fields into the diagnostic routine (Figure 5, bottom). Some discrepancies as large as 0.5 Sv exist at $\sigma < 25$, but the overall water mass subduction curve is well reproduced. Thus the first term on the right-hand side of equation (4) is the dominant term in the time-mean subduction rate. The integrand of this term, $-(\bar{w}_H + \bar{\mathbf{u}}_H \cdot \nabla H)$, is plotted in Figure 6. Small-scale variations in the maximum mixed-layer depth and the horizontal circulation field lead to locally intense volume fluxes. Lateral induction across the small-scale features of $\nabla H$ subducts water at rates up to 300 m/yr. In contrast, the vertical velocity field at the mixed-layer base is predominantly large-scale. It is confirmed that when the volume flux field of Figure 6 is integrated over $\overline{\mathcal{A}_H}$, the result is the "annual" subduction rate in Figure 5.

### 4.2. Eddy Subduction Rates

[26] Section 2 outlined two kinematic methods to compute eddy subduction rates. First, we diagnose the eddy subduction rate across the maximum depth of the mixed layer, as defined by equation (4). The second integral on the right hand side, $\overline{\int^{\mathcal{A}'_H(\sigma,t)} - (w_H + u_H \cdot \nabla H) d\mathcal{A}}$, is the subduction due to the time-variable density and velocity fields, defined here as one version of the eddy subduction rate. This term cannot be easily shown in a geographical picture. The magnitude of this term, however, is deduced from the differences between the subduction rate calculated with annual mean fields and 10-day average fields. This calculation shows that the eddy subduction rate is less than 1 Sv at all densities.

[27] Another kinematic method is to compute the contribution of eddies to $\overline{S_h}(\sigma)$ rather than $\overline{S_H}(\sigma)$. In particular, this method allows a time-variable mixed-layer depth and an eddy volume flux across this surface (the second integral of the R.H.S. of equation (3)). In the state estimate fields, the integrand, $\overline{-(\partial h'/\partial t + \mathbf{u}'_h \cdot \nabla h')}$, is dominated by the seasonal cycle and does not allow the impact of mesoscale eddies to be clearly diagnosed.

[28] As a remedy, a different decomposition of the mean and eddy components of the circulation is sought. The effective subduction period, $\tau_{eff}$, is defined to be the time period over which permanent subduction occurs. Using the diagnostic method of *Marshall et al.* [1993], the domain-averaged period of effective subduction is 53 days beginning on 23 February 1993. By definition, the time-mean subduction can be diagnosed by averaging solely over the effective subduction period. In the short time period of effective subduction, the seasonal cycle can be approximated by a linear trend. Using a mean over the effective subduction

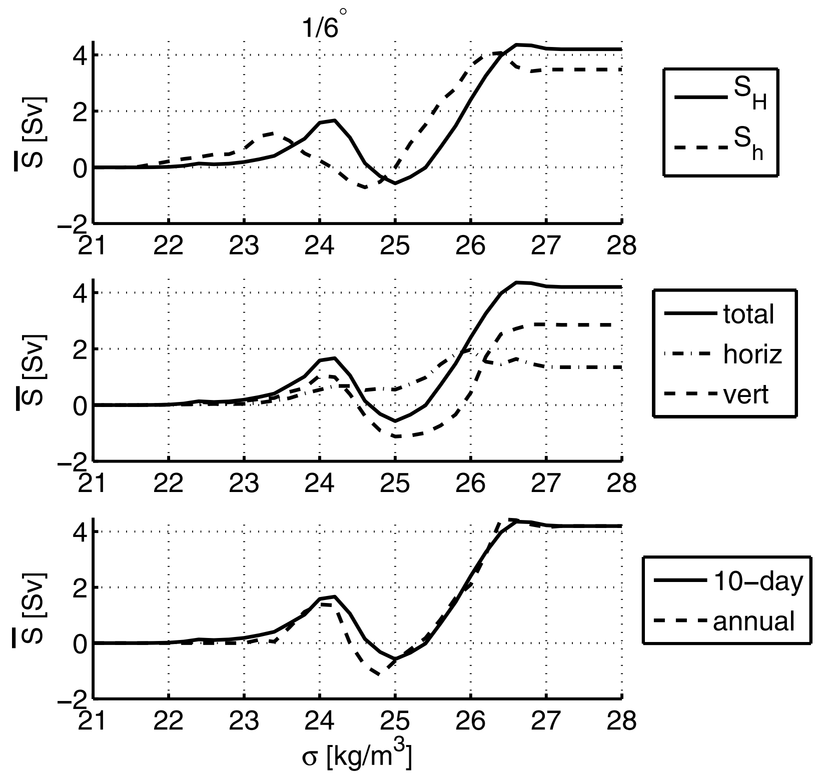


**Figure 5.** (top) Water mass subduction rates across the maximum mixed-layer depth ($\overline{S_H}$) and the time-variable mixed-layer base ($\overline{S_h}$) in the 1/6° state estimate. The subduction rates are computed directly from velocity and density fields. (middle) Decomposition of the water mass subduction rate into the part due to lateral induction ("horiz") and vertical velocity ("vert"). The full subduction rate is also plotted ("total"). (bottom) Water mass subduction rate across the maximum mixed-layer depth computed with 10-day average fields and annual mean fields.

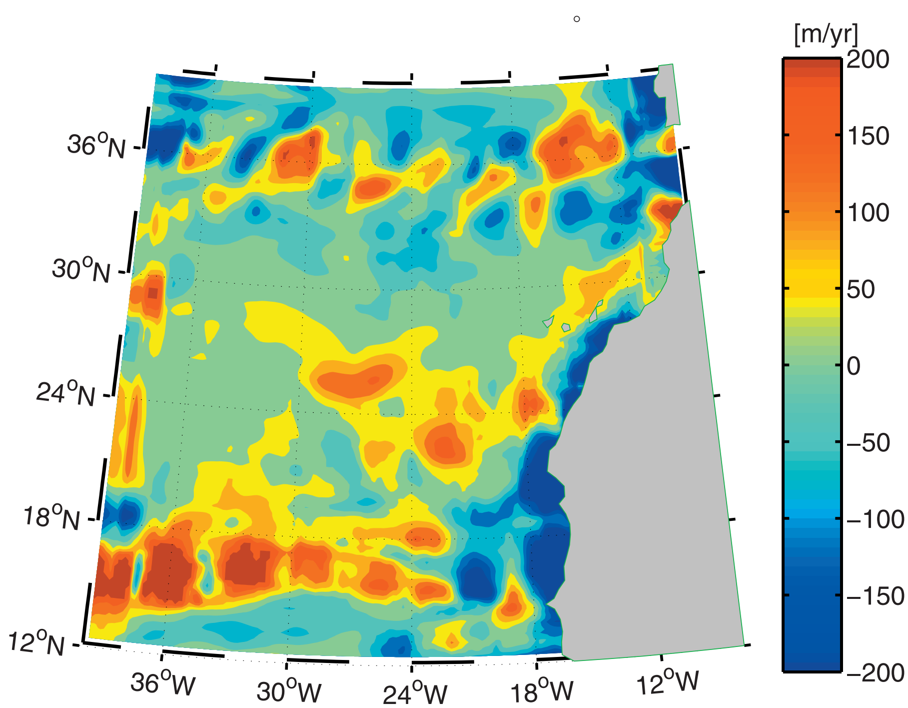


**Figure 6.** Local subduction rate calculated from annual-mean fields. The velocity and mixed-layer depth fields have been smoothed with a 1° running filter.

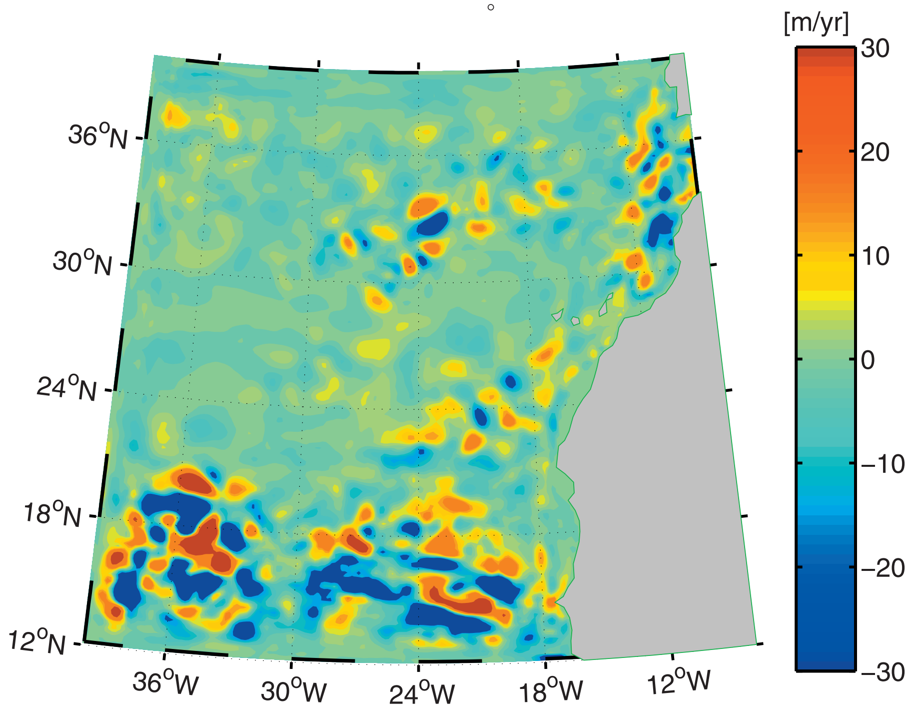


**Figure 7.** Mean eddy-volume flux across the time-variable mixed-layer base. Note the color scale ranges from −30 m/yr to 30 m/yr, a smaller range than Figure 4.

period and anomalies defined relative to the linear-trend seasonal cycle, the eddy volume flux, $-(\partial h'/\partial t + \overline{\mathbf{u}_h' \cdot \nabla h'})$, is recomputed. Instantaneous eddy volume fluxes are larger than 200 m/yr in localized regions. The eddy volume fluxes are scaled by the efficiency of subduction, $\epsilon = \tau_{eff}/\tau$, the percentage of time in which subduction is permanent, and plotted in Figure 7. Scaled eddy volume fluxes as large as 40 m/yr are present in the North Equatorial Current and in parts of the Azores Current. When integrated over the mean isopycnal surfaces, however, the small-scale features are largely offsetting and the water mass subduction rate due to eddy volume fluxes is small. In this calculation, the effective subduction period is considered uniform for the entire domain, which is not strictly true because the subduction period increases toward the tropics. Changing the effective subduction period leads to shifts in the locations of the features in Figure 7, but the integrated water mass subduction is not sensitive to this assumption.

### 4.3. Subduction and Spatial Resolution

[29] Although the contribution to subduction by the time-variable circulation was small in an integrated sense, the small-scale features of Figures 6 and 7 lead us to investigate the impact of spatial resolution on the diagnosed subduction rate. The availability of a twin, 2° resolution state estimate allows us to repeat the previous calculations with the coarse-resolution estimate (Figure 8). Both state estimates are constrained to have large-scale circulations which satisfy the regional observations. The 2° subduction rate can be well-described by splitting the water masses into light ($\sigma <$ 25) and heavy ($\sigma >$ 25) categories. 5 Sv of heavy water is subducted and 1 Sv of light water is obducted, for a domain-averaged net 4 Sv of subduction. The ratio of subduction in the horizontal to vertical is altered in the 2° estimate such that lateral induction is now the greater contributor, indicating that the representation of ocean processes may be resolution dependent.

[30] The difference in subduction between the 2° and 1/6° state estimates is plotted in Figure 9 for both a fixed and time-variable mixed-layer base. The domain-integrated subduction, $\bar{S}(\sigma_{\max})$, differs by less than 0.5 Sv, but in specific density bands, the difference is 2–3 Sv ($23.8 < \sigma < 24.2$ and $25.8 < \sigma < 26.2$). These density bands are consistent with the maximum eddy kinetic energy regions of the northeast Atlantic, with the Azores Current outcrop isopycnal at $\sigma \approx 26$ kg/m$^3$ and the North Equatorial Current at $\sigma \approx 24$ kg/m$^3$. To more fully interpret the differences between the state estimates at different resolution, we next explore the processes that lead to subduction in the two complementary estimates. In addition, we evaluate whether the eddy subduction rate can be reliably diagnosed by the thermodynamic method.

### 4.4. Thermodynamic Estimates of Subduction

[31] The thermodynamic equation for subduction (equation (8)) is applied to the state estimate with the bottom boundary fixed at the maximum depth of the mixed layer, $H(x, y)$. The annual-mean, surface-layer open boundary volume flux, $\overline{M_B}(\sigma)$, is calculated with 10-day average fields. No standard climatology for open-ocean velocity exists, but as a first guess, the ECCO global state estimate time-variable velocity field is mapped onto the regional boundaries (Figure 10, "ECCO Global Est."). The northeast Atlantic state estimate provides a better estimate of the open-boundary velocity by adjusting all the open boundary fields until consistency with regional observations is found

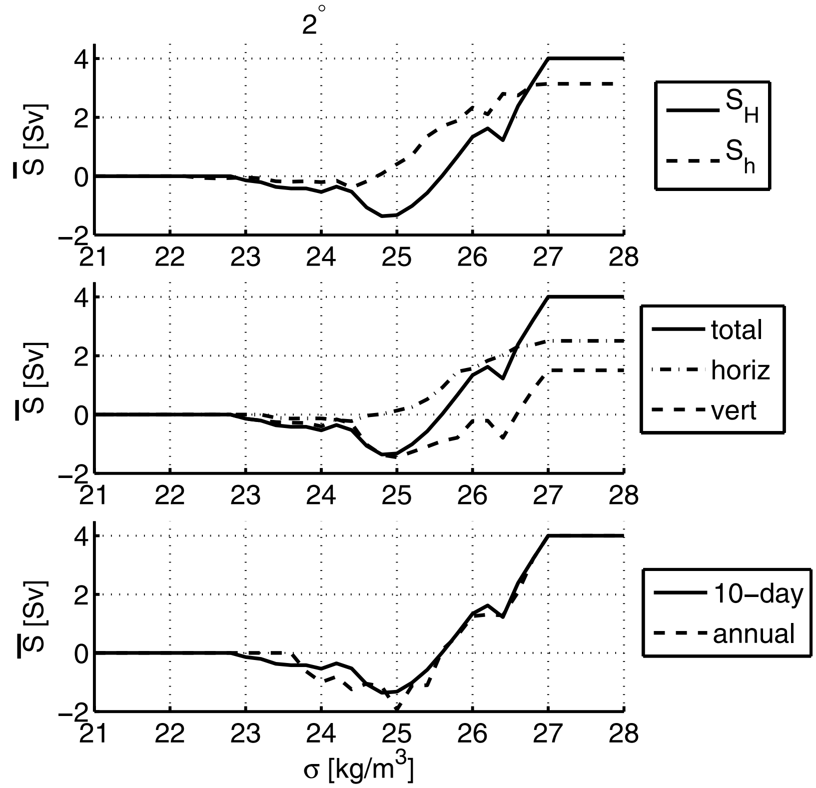


**Figure 8.** In the same format as Figure 5, but using density and velocity fields from the 2° state estimate.

(Figure 10, "N.E. Atl. Est."). The global state estimate has 2° resolution, and to make a fair comparison, we have computed $\overline{M_B}$ for the 2° regional state estimate. Both circulation estimates show that light ($\sigma$ < 24) water is expelled from the basin primarily in the uppermost 50 m of the North Equatorial Current. The ECCO estimate has too much light water, and the data constraint of the NE Atlantic estimate corrects for this bias. Both estimates also show that there is a net source of volume through the boundary, with the majority of incoming water in the heavier density class 24.2 < $\sigma$ < 26.5, signifying the lateral recirculation of the mode waters of the subtropical gyre. The NE Atlantic state estimate has a significant difference from the ECCO estimate, however. The regional data require a

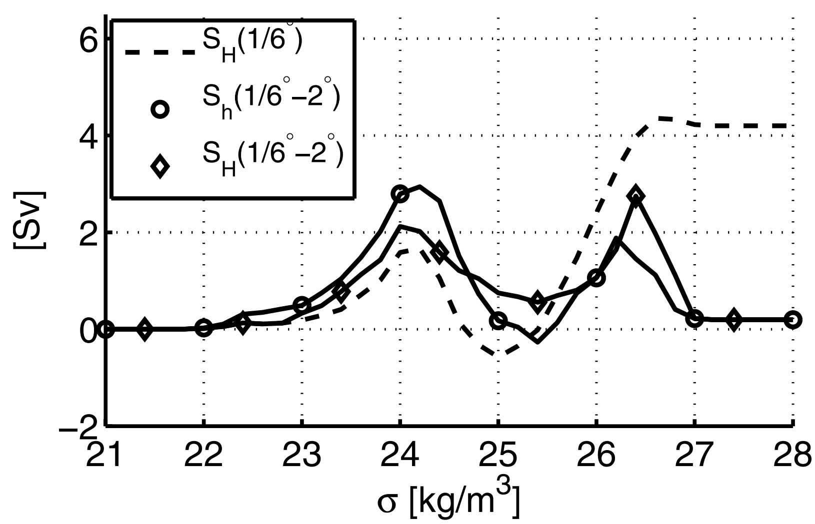


**Figure 9.** Comparison of the subduction rates in the 1/6° and 2° state estimates. Solid line with circles: Difference in subduction rates calculated across the time-variable mixed-layer base. Solid line with diamonds: Difference in subduction rate calculated across the maximum mixed-layer depth. The 1/6° total subduction rate (dashed line) is plotted for reference.

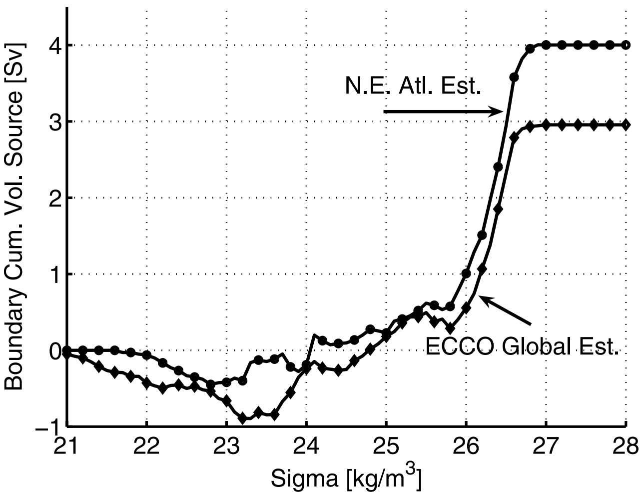


**Figure 10.** Open boundary source of volume to the surface layer in the first-guess circulation from the ECCO coarse-resolution global estimate, and the improved circulation from a northeast Atlantic state estimate. $\overline{M_B}(\sigma)$ is the annual average source of volume at all densities less than $\sigma$. Solid line denotes the calculation for density bins of $\Delta\sigma$ = 0.1, and circles and diamonds are for density bins of $\Delta\sigma$ = 0.2.

25% increase in the domain-integrated boundary volume source, and this difference directly sets the domain-integrated subduction by conservation of mass in the upper ocean.

[32] The water masses supplied by the boundary are subject to transformation by air-sea fluxes. A first guess of the air-sea transformation rate, $F_S(\sigma, t)$, is calculated with 10-day average NCEP Reanalysis air-sea fluxes [*Kalnay et al.*, 1996] and 10-day averages of modeled SST at 1/6° resolution following the method of *Speer and Tziperman* [1992]. The annual-mean air-sea transformation rate, $\overline{F_S}(\sigma)$, is the time-mean of the 10-day averages (see Figure 11, top left). This approach shows that air-sea fluxes make subtropical surface waters more dense, $\overline{F_S}(\sigma) > 0$. Splitting the surface buoyancy flux into two parts, $\overline{F_{heat}}(\sigma)$ for the heat flux component and $\overline{F_{salt}}(\sigma)$ for the buoyancy flux by evaporation and precipitation, shows that the $\overline{F_{salt}}(\sigma)$ term makes the surface water more dense, and that the domain-integrated heat fluxes are close to zero.

[33] The first-guess air-sea fluxes are imposed upon the model without regard to the sea surface temperature and salinity. Air-sea transformation, however, depends not only upon the air-sea fluxes, but upon the sea surface density as well. To quantify the impact of a different sea surface density field, we calculate $\overline{F_{salt}}(\sigma)$ with the NCEP fluxes and the 2° resolution ocean fields (compare the top left and bottom left plots in Figure 11). Around the density range $\sigma$ = 24, the 2° estimate shows 1 Sv of additional transformation by heat flux, but no significant changes in other density bands. The sensitivity of these results to time resolution can also be computed. When using annual-mean fluxes and surface fields, we find transformation rates that are smaller by up to 50% especially in the summer outcrop densities.

[34] The mooring meteorological measurements of the Subduction Experiment showed that the NCEP product underestimates the net heat gain of the ocean [*Moyer and Weller*, 1995; *Weller et al.*, 2004]. A better estimate of air-sea transformation is available with the northeast Atlantic state estimate, where air-sea fluxes and sea surface density are available in a dynamically consistent framework, and fluxes are adjusted for consistency with regional observations. Point values of NE Atlantic heat flux are adjusted up to 70 W/m$^2$, but the domain-integrated heat flux is only changed by 5 W/m$^2$ from the NCEP Reanalysis (see Figure 11; compare $\overline{F_{heat}}(\sigma)$ in the top left and top right plots, for example). This small domain-integrated change in heat flux due to the observational constraints is similar in both the 2° and 1/6° experiments. In a future study, the Subduction Experiment meteorological buoy observations could be used to directly constrain the circulation, while only ocean observations were used here.

[35] Measurements of open-ocean freshwater fluxes are even more difficult to acquire than heat fluxes, and are potentially more uncertain. The regional-average adjustment in the surface freshwater flux by state estimation is $1.1 \times 10^8$ m/s (see Figure 11; compare $\overline{F_{salt}}(\sigma)$ in the top left and top right plots). The amount of evaporation is significantly altered from the NCEP Reanalysis, where the mean evaporation rate is $3 \times 10^8$ m/s. The NE Atlantic state estimate makes changes to the freshwater flux which increase the overall air-sea transformation by 2–3 Sv. The domain-integrated adjustments to NCEP freshwater flux have a similar sign and magnitude whether the model has 2° or 1/6° resolution, but the adjustments at 2° are larger in the light density classes (compare bottom left and bottom right plots in Figure 11). Overall, the implied large changes in freshwater flux, and their dependence upon spatial resolution, are indicative that this component of transformation is somewhat unconstrained.

[36] What is the relative importance of the open-boundary volume source and air-sea transformation on the properties of subducted water? Equation (8) gives the framework for comparing the two, but it also requires an estimate of transformation by the interior ocean physics ($F_D(\sigma, t)$) and boundary effects ($F_B(\sigma, t)$), and an estimate of the interannual variability ($\partial V(\sigma, t)/\partial t$). The calculation for $F_D(\sigma, t)$ uses the same grid and discretization scheme as the numerical model, but is calculated offline, which makes it an imperfect reconstruction. In Figure 12, $\overline{F_B}(\sigma)$ has not been plotted because its maximum value is approximately 0.5 Sv.

[37] An integrated picture of the processes behind subduction for the years 1992–1993 is seen in Figure 12. The open boundaries are a net source of waters at a wide range of densities and surface freshwater fluxes, primarily through evaporation, increased the density of the surface waters. Much of the newly dense water is stored in the surface layer, and a longer time series would be necessary to distinguish how episodic or anomalous the storage is. A portion of newly dense water, especially in the range $25.5 < \sigma < 26.5$ is ultimately subducted into the main thermocline. Diffusive processes are nonnegligible in the density range of greatest subduction, but further interpretation of the structure of $F_D(\sigma, t)$ is outside the scope of this work [see *Tandon and Zahariev*, 2001].

[38] The thermodynamic estimate of subduction relies upon the reconstruction of the volume and buoyancy budgets of the upper ocean. The error in the reconstruction is calculated by comparing the thermodynamic and kine-

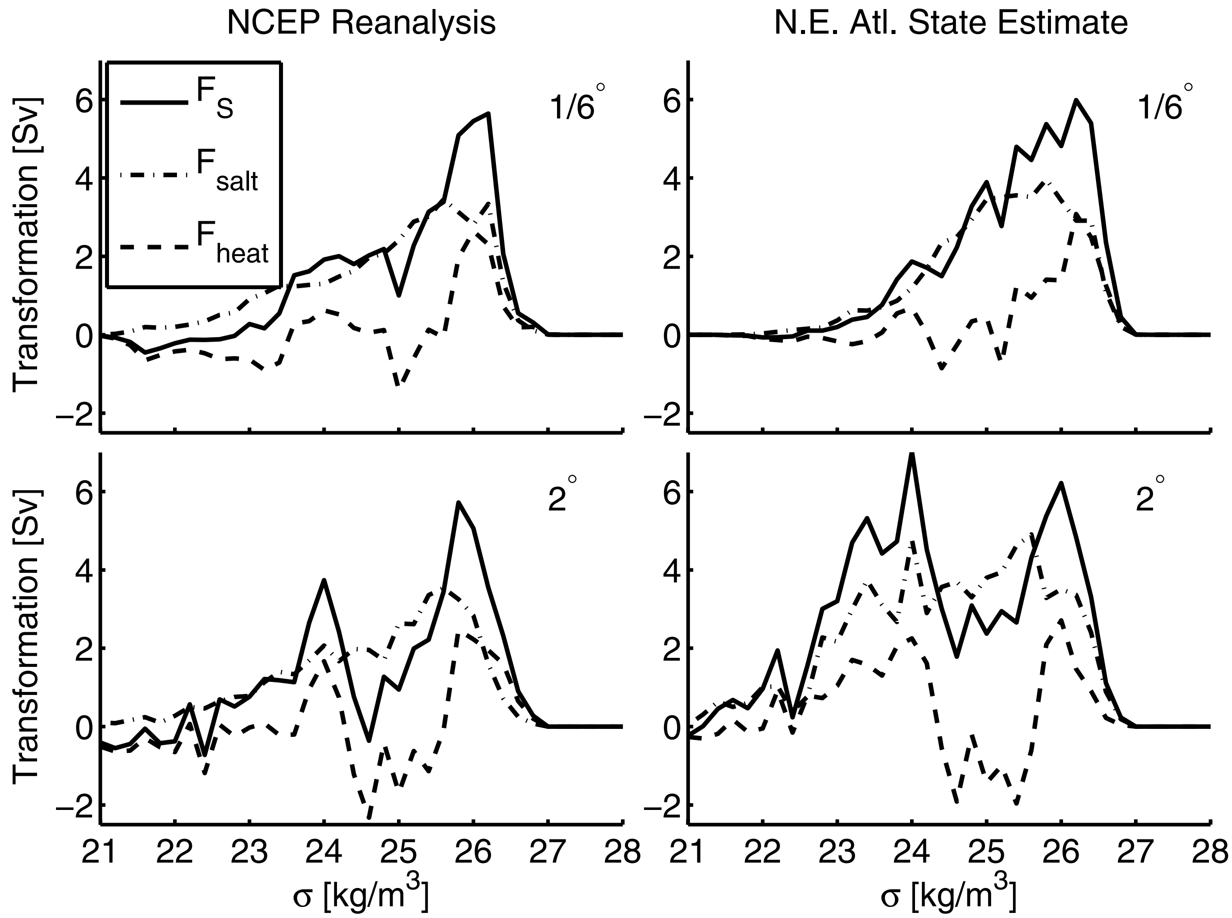


**Figure 11.** Annual-average air-sea transformation rates computed from (left) 10-day fields of NCEP Reanalysis air-sea and (right) air-sea fluxes adjusted by state estimation using sea surface density (top) from the 1/6° northeast Atlantic state estimate and (bottom) computed for the 2° state estimate. Bold, solid line denotes annual-average air-sea transformation rate, $\overline{F_S}(\sigma)$. The contribution by freshwater fluxes, $\overline{F_{salt}}(\sigma)$ (dash-dotted line) and contribution by heat fluxes, $\overline{F_{heat}}(\sigma)$ (dashed line), are also plotted.

matic subduction rates (see bottom plot, Figure 12). The error has a standard deviation of roughly 1 Sv. All budgets are subject to errors due to the binning of density classes [see *Marshall et al.*, 1999, Appendix B]. To assess this error, the thermodynamic subduction rate is also calculated with density bins of $\Delta\sigma = 0.1$ and $\Delta\sigma = 0.2$. The standard deviation of the difference is 0.3 Sv, too small to explain the residual of the thermodynamic method. Another source of error is the diffusion term of the buoyancy budget. Here we compute diffusion offline with a constant diffusivity, as the mixed-layer diffusivities calculated by the KPP model are too memory-intensive to be stored. $\overline{F_D}(\sigma)$ reduces the standard deviation of the error in the thermodynamic budget, but only by 0.1 Sv. The diagnosed diffusive fluxes correctly act to densify light waters and lighten dense waters, but the remaining residual suggests that the diffusive fluxes are underestimated. *Nurser et al.* [1999] showed that entrainment mixing is significant and that time-dependent mixed-layer diffusivities are necessary to quantify this process. On the basis of this evidence, the bulk of the error in the thermodynamic estimate is likely due to the offline calculation of the buoyancy budget and therefore a thermodynamic estimate of eddy subduction is not attempted at this time.

## 5. Summary and Discussion

[39] An accurate quantification of subduction requires knowledge of the time-variable three-dimensional circulation and the gradients of those fields. Observations alone, even those from intensive field experiments such as the Subduction Experiment, are insufficient. When considering a regional model simulation, on the other hand, water mass budgets show that subduction is dependent upon both open-boundary velocities and air-sea fluxes: two quantities which are highly uncertain in the open ocean. A novel approach to solve the data inadequacy problem and the model uncertainty problem is to combine observations and a model to form a state estimate, as detailed in a companion paper [*Gebbie et al.*, 2006]. The state estimate serves as a dynamical interpolator of the observations, giving a high-resolution estimate which is consistent with the data. Also, the state estimate accounts for the uncertainty in the lateral and surface boundary conditions by adjusting them within reasonable bounds as required by the observations. The

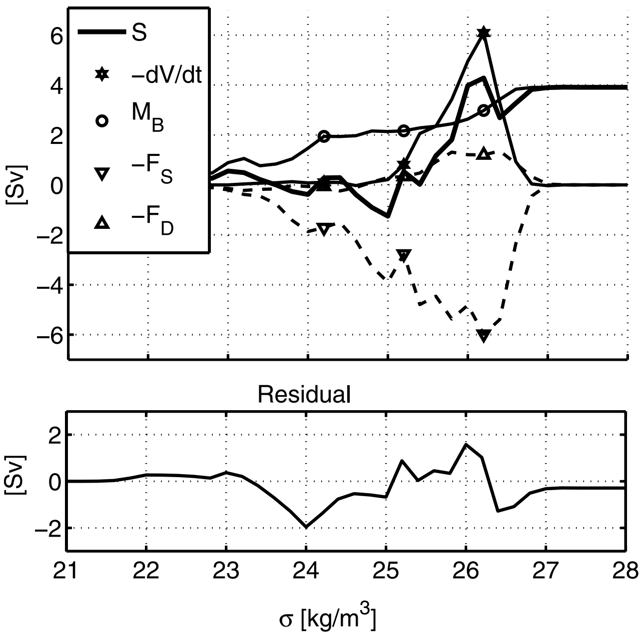


**Figure 12.** (top) Thermodynamic calculation of annual-average water mass subduction rate, $\overline{S}(\sigma)$. The properties of subducted water are determined by isopycnal storage ($\partial V(\sigma)/\partial t$, stars), the open-boundary volume source ($\overline{M_B}(\sigma)$, circles), air-sea transformation ($\overline{F_S}(\sigma)$, downward triangles), and transformation by diffusive processes ($\overline{F_D}(\sigma)$, upward triangles). (bottom) The residual is the difference between the subduction rates calculated by kinematic and thermodynamic methods.

final product is a three-dimensional, time-evolving circulation that is self-consistent with the equations of motion. A first-guess model simulation, on the other hand, had a grossly erroneous upper ocean hydrography which was not suitable for quantitative analysis.

[40] Using the state estimate, the role of eddies in subducting water into the main thermocline is diagnosed. In the northeast Atlantic Ocean, eddy subduction, defined as the contribution to subduction by the time-variable density and velocity fields, is less than 1 Sv in all density classes. In two density classes centered around $\sigma$ = 24 and $\sigma$ = 26, however, small-scale features subduct 2–3 Sv. The Azores Current and the North Equatorial Current are generally consistent with these density classes, and have been suggested as potential sites of eddy subduction by previous investigators [*Spall*, 1995; *Robbins et al.*, 2000] owing to their frontal structure and enhanced eddy kinetic energy. When taking a time average over a short period of time, such as the 1–2 years of the Subduction Experiment, much of the signature of mesoscale eddies remains in the time-mean fields. For this reason, we hypothesize that the results of this study are strongly affected by the short available record length and the averaging assumptions that must be made.

[41] The dependence of the diagnosed subduction rates on the spatial resolution of the state estimate suggests that uncertainties in both small-scale processes and open-ocean surface fluxes are important. The differences in subduction between the coarse-resolution and eddy-permitting state estimates may be interpreted as the error incurred by using a coarse-resolution model, since both estimates use the same observational information. A scaling argument can be used to estimate the timescale over which this error significantly biases water mass properties. The simple scaling is $\tau = V/\Delta S$, where $\tau$ is the timescale, $V$ is the volume in a particular density class below the surface layer, and $\Delta S$ is the difference in water mass subduction rate across the density range. Plugging in the maximum difference in subduction rate of $\Delta S$ = 2 Sv for 25.5 < $\sigma$ < 26.5 and the corresponding water mass volume ($V \approx$ 3000 km × 3000 km × 100 m depth), the timescale is 10–20 years.

[42] *Marshall* [1997] showed that eddy subduction occurs by transport of the so-called "bolus" velocity. Eddy parameterization schemes are already capable of predicting this advective component of eddy flux, but it is uncertain how well they work in the oceanic mixed layer. Coarse-resolution models with eddy parameterization schemes, such as the study of *Spall et al.* [2000], seem to predict eddy subduction rates on the order of 10 m/yr in the northeast Atlantic, significantly lower than the 40 m/yr eddy volume fluxes calculated here. Future work should check the adequacy of eddy parameterization schemes in a more detailed way, with particular focus on eddy–mixed-layer interaction.

[43] Even with only 2 years of Subduction Experiment observations, the methodology of state estimation is able to produce an estimate of the magnitude of eddy subduction. Nevertheless, a major difficulty in this study is the short observational record in the northeast Atlantic. Model simulations frequently take 20 years before a spatially coherent eddy subduction signal is found. In general, the decomposition of the circulation into mean and eddy components is troublesome in this region because of the lack of a stable mean velocity field. Considering the zonal velocity time series from a 1° North Atlantic state estimate [*Stammer et al.*, 2002], at least 10 years of data are needed for a stable mean in this region. *Müller and Siedler* [1992] have commented that variability in the 4–6 year frequency band is responsible for the unstable means. A longer time series will allow a better decomposition of permanent and temporary subduction, and will allow the investigator to more confidently rule out model drift as an artifact in the state estimate. A complete study of eddy subduction, therefore, will likely require a spatially dense, 10- to 20-year observational record.

## Appendix A: Derivation of the Eddy Subduction Rate

[44] The eddy subduction rate, as defined by *Marshall* [1997], can be translated to the notation of this work. First, define $\overline{\mathcal{A}_h}(\sigma)$ to be the surface defined by the base of the time-mean mixed layer with time-mean density less than $\sigma$. A useful mathematical shorthand is

$$\int^{\mathcal{A}'_h(\sigma,t)} (\cdot) d\mathcal{A} = \int^{\mathcal{A}_h(\sigma,t)} (\cdot) d\mathcal{A} - \int^{\overline{\mathcal{A}_h}(\sigma)} (\cdot)\, d\mathcal{A}, \qquad \text{(A1)}$$

so that the integral over $\mathcal{A}'_h(\sigma, t)$ represents the effect of the time-variable mixed-layer depth and density. Then the water mass subduction rate, equation (2), can be rewritten:

$$S_h(\sigma,t) \equiv \int^{\overline{\mathcal{A}_h}(\sigma)+\mathcal{A}'_h(\sigma,t)} s(x,y,t)d\mathcal{A}. \tag{A2}$$

[45] Now take the time mean, denoted by the overbar:

$$\overline{S_h}(\sigma) = \overline{\int^{\overline{\mathcal{A}_h}(\sigma)} s(x,y,t)d\mathcal{A}} + \overline{\int^{\mathcal{A}'_h(\sigma,t)} s(x,y,t)d\mathcal{A}}. \tag{A3}$$

[46] Using the definition of $s(x, y, t)$, equation (1), we can find an expression for $\overline{s(x,y,t)}$ and expand the first term of the right-hand side into two terms:

$$\begin{aligned}\overline{S_h}(\sigma) = & \int^{\overline{\mathcal{A}_h}(\sigma)} -\left(\bar{w}_h + \bar{\mathbf{u}}_h \cdot \nabla\bar{h}\right)d\mathcal{A} \\ & + \int^{\overline{\mathcal{A}_h}(\sigma)} -\left(\frac{\partial h'}{\partial t} + \overline{\mathbf{u}'_h \cdot \nabla h'}\right)d\mathcal{A} \\ & + \overline{\int^{\mathcal{A}'_h(\sigma,t)} s(x,y,t)d\mathcal{A}}. \end{aligned} \tag{A4}$$

This is the decomposition of the subduction rate presented as equation (3) in the text, with the last two terms representing the water mass eddy subduction rate. In the work of *Marshall* [1997], the term which corresponds to the third term of (A4) has a slightly different form. Instead of $s(x, y, t)$, *Marshall* [1997] found $s'(x, y, t)$. With the definitions presented here, $s(x, y, t)$ is correct because the integral $\int^{\mathcal{A}'_h(\sigma,t)} \overline{s(x,y,t)}\, d\mathcal{A}$ need not vanish.

## Appendix B: Diagnostics for a z-Coordinate State Estimate

[47] Isopycnal analysis of the z-coordinate (or "level coordinate") state estimate follows the numerical model analysis in Appendices A and B of *Marshall et al.* [1999]. Here the diagnostics are extended to calculate the volume flux through the surface layer base and the open boundaries. The base of the control volume can be time-variable or fixed with appropriate adjustments made to the diagnostic routine. Outside of the regional boundaries, set $H(x, y) = 0$. The volume flux at density less than $\sigma$ across the surface defined by $H(x, y)$ is $M(\sigma, t)$. There are two sources to $M(\sigma, t)$:

$$M(\sigma,t) = M_B(\sigma,t) - S(\sigma,t), \tag{B1}$$

the volume flux across the lateral boundary, $M_B(\sigma, t)$, and the volume flux across the horizontally varying bottom boundary, $S(\sigma, t)$. When diagnosed on the C-grid of the MITgcm and state estimate,

$$\begin{aligned} M(\sigma,t) = & \Sigma_{ijk} \quad u(i,j,k,t)\cdot a_{yz}(i-1/2,j,k)\cdot \Pi_{ML_u}(\sigma_n,i,j,k,t) \\ & + \Sigma_{ijk} \quad v(i,j-1/2,k,t)\cdot a_{xz}(i,j-1/2,k) \\ & \cdot \Pi_{ML_v}(\sigma_n,i,j,k,t) + \Sigma_{ijk} \quad w(i,j,k-1/2,t)\cdot a_{xy}(i,j) \\ & \cdot \Pi_{ML_w}(\sigma_n,i,j,k,t), \end{aligned} \tag{B2}$$

where $a_{xy,xz,yz}$ is the area of the respective grid face and $\Pi_{MLu,v,w}$ is a boxcar function. The velocity is defined on a staggered grid relative to the tracer and density fields. Hence coordinates with 1/2 refer to grid faces, not the center of grid cells. Density values must be interpolated to grid faces, and a simple linear scheme is used here. From above, the boxcar function, $\Pi_{MLu}$, for example, is defined by

$$\Pi_{ML_u}(\sigma_n,i,j,k,t) = \left\{\begin{array}{lll} 1 & if & \left\{\begin{array}{c}\sigma\left(i-\frac{1}{2},j,k,t\right) < \sigma_n \\ H(i-1,j) \le z(k) < H(i,j)\end{array}\right) \\ -1 & if & \left\{\begin{array}{c}\sigma\left(i-\frac{1}{2},j,k,t\right) < \sigma_n \\ H(i-1,j) > z(k) \ge H(i,j)\end{array}\right) \\ 0 & & otherwise \end{array}\right). \tag{B3}$$

Boxcar functions for the other components of velocity follow in a similar way.

[48] $S(\sigma, t)$ must still be isolated from $M(\sigma, t)$. Replace the full velocity field with the open boundary velocity field, $(u, v, w) = (u_B, v_B, 0)$, and reevaluate equation (B2) to estimate the open boundary volume flux, $M_B(\sigma, t)$. Then the water mass subduction rate is deduced by subtraction (equation (B1)).

[49] **Acknowledgments.** Carl Wunsch and Patrick Heimbach served as my graduate school coadvisors and could rightfully be coauthors on this work, although I do not wish to blame them for any remaining errors. Amit Tandon inspired the approach of this paper. John Marshall, Eli Tziperman, and Laure Zanna contributed many useful comments. Funding for this work has been primarily through a NASA Earth System Science Fellowship. This work was also partially funded by the NSP paleoclimate program, grant ATM-0502482. Detlef Stammer was instrumental in acquiring computer time at the San Diego Supercomputer Center, the University of Texas, and the Naval Oceanographic Office MSRC at Stennis Space Center. Daniel Jamous supplied the FORTRAN water mass diagnostics which were later translated to MATLAB. The previous 8+ years of work by the ECCO Consortium allowed this research to happen. Two anonymous reviewers greatly clarified and improved this work.

## References

Brink, N. J., K. A. Moyer, R. P. Trask, and R. A. Weller (1995), The Subduction Experiment: Mooring field program and data summary, technical report, Woods Hole Oceanogr. Inst., Woods Hole, Mass.

Cushman-Roisin, B. (1987), Subduction, in *Aha Huliko'a Proceedings of the University of Hawai'i*, edited by P. Muller and D. Henderson, pp. 181–196, Univ. of Hawai'i at Manoa, Honolulu.

Donners, J., S. S. Drijfhout, and W. Hazeleger (2005), Water mass transformation and subduction in the South Atlantic, *J. Phys. Oceanogr.*, *35*, 1841–1860.

Follows, M. J., and J. C. Marshall (1994), Eddy driven exchange at ocean fronts, *Ocean Modell.*, *102*, 5–9.

Garrett, C., and A. Tandon (1997), The effects on water mass formation of surface mixed layer time-dependence and entrainment fluxes, *Deep Sea Res., Part I*, *44*, 1991–2006.

Garrett, C., K. Speer, and E. Tragou (1995), The relationship between water mass transformation and the surface buoyancy flux, with application to Phillips' Red Sea model, *J. Phys. Oceanogr.*, *25*, 1696–1705.

Gebbie, G. (2004), Subduction in an eddy-resolving state estimate of the northeast Atlantic Ocean, Ph.D. thesis, Mass. Inst. of Technol./Woods Hole Oceanogr. Inst. Joint Program in Oceanogr., Cambridge, Mass.

Gebbie, G., P. Heimbach, and C. Wunsch (2006), Strategies for nested and eddy-permitting state estimation, *J. Geophys. Res.*, *111*, C10073, doi:10.1029/2005JC003094.

Hazeleger, W., and S. S. Drijfhout (2000), Eddy subduction in a model of the subtropical gyre, *J. Phys. Oceanogr.*, *29*, 266–288.

Jenkins, W. J. (1987), H-3 and he-3 in the beta-triangle: Observations of gyre ventilation and oxygen utilization rates, *J. Phys. Oceanogr.*, *17*, 763–783.

Jia, Y. (2000), Formation of an Azores Current due to Mediterranean overflow in a modelling study of the North Atlantic, *J. Phys. Oceanogr.*, *103*, 2342–2358.

Joyce, T. M., J. R. Luyten, A. Kubryakov, F. B. Bahr, and J. S. Pallant (1998), Meso- to large-scale structure of subducting water in the subtro-

pical gyre of the eastern North Atlantic Ocean, *J. Phys. Oceanogr.*, *28*, 40–61.
Kalnay, E., et al. (1996), The NCEP/NCAR 40-year reanalysis project, *Bull. Am. Meteorol. Soc.*, *77*, 437–440.
Large, W. G., and A. J. G. Nurser (2001), *Ocean Surface Water Mass Transformation*, *Int. Geophys. Ser.*, vol. 77, pp. 317–336, Academic, San Diego, Calif.
Large, W. G., J. C. McWilliams, and S. C. Doney (1994), Oceanic vertical mixing: A review and a model with a nonlocal boundary layer parameterization, *Rev. Geophys.*, *32*, 363–403.
LeDimet, F.-X., and O. Talagrand (1986), Variational algorithms for analysis and assimilation of meteorological observations: Theoretical aspects, *Tellus, Ser. A*, *38*, 97–110.
Levitus, S., and T. Boyer (1994), *World Ocean Atlas 1994*, vol. 4, *Temperature, NOAA Atlas NESDIS 4*, Natl. Oceanic and Atmos. Admin., Silver Spring, Md.
Marotzke, J., R. Giering, K. Q. Zhang, D. Stammer, C. Hill, and T. Lee (1999), Construction of the adjoint MIT ocean general circulation model and application to Atlantic heat transport sensitivity, *J. Geophys. Res.*, *104*, 529–547.
Marshall, D. (1997), Subduction of water masses in an eddying ocean, *J. Mar. Res.*, *55*, 201–222.
Marshall, J. C., and A. J. G. Nurser (1991), A continuously stratified thermocline model incorporating a mixed layer of variable thickness and density, *J. Phys. Oceanogr.*, *21*, 1780–1792.
Marshall, J. C., A. J. G. Nurser, and R. G. Williams (1993), Inferring the subduction rate and period over the North Atlantic, *J. Phys. Oceanogr.*, *23*, 1315–1329.
Marshall, J., A. Adcroft, C. Hill, L. Perelman, and C. Heisey (1997), A finite volume, incompressible Navier-Stokes model for studies of the ocean on parallel computers, *J. Geophys. Res.*, *102*, 5753–5766.
Marshall, J., D. Jamous, and J. Nilsson (1999), Reconciling thermodynamic and dynamic methods of computation of water-mass transformation rates, *Deep Sea Res., Part I*, *46*, 545–572.
Moyer, K. A., and R. A. Weller (1995), Observations of surface forcing from the Subduction Experiment: A comparison with global model products and climatological datasets, *J. Clim.*, *10*, 2725–2742.
Müller, T. J., and G. Siedler (1992), Multi-year time series in the eastern North Atlantic Ocean, *J. Mar. Res.*, *50*, 63–98.
Nakamura, N. (1995), Modified Lagrangian-mean diagnostics of the stratospheric polar vortices. Part I. Formulation and analysis of GFDL, SKYHI GCM, *J. Atmos. Sci.*, *52*, 2096–2108.
New, A. L., Y. Jia, M. Coulibaly, and J. Dengg (2001), On the role of the Azores current in the ventilation of the North Atlantic Ocean, *Prog. Oceanogr.*, *48*, 163–194.
Nurser, A. J. G., R. Marsh, and R. G. Williams (1999), Diagnosing water mass formation from air-sea fluxes and surface mixing, *J. Phys. Oceanogr.*, *29*, 1468–1487.
Robbins, P. E., J. F. Price, W. B. Owens, and W. J. Jenkins (2000), The importance of lateral diffusion for the ventilation of the lower thermocline in the subtropical North Atlantic, *J. Phys. Oceanogr.*, *30*, 67–89.
Rudnick, D. L., and J. R. Luyten (1996), Intensive surveys of the Azores Front. Part I: Tracers and dynamics, *J. Geophys. Res.*, *101*, 923–939.
Spall, M. A. (1995), Frontogenesis, subduction, and cross-front exchange at upper ocean fronts, *J. Geophys. Res.*, *100*, 2543–2557.
Spall, M. A., R. A. Weller, and P. W. Furey (2000), Modeling the three-dimensional upper ocean heat budget and subduction rate during the Subduction Experiment, *J. Phys. Oceanogr.*, *30*, 26,151–26,166.
Speer, K., and E. Tziperman (1992), Rates of water mass formation in the North Atlantic Ocean, *J. Phys. Oceanogr.*, *22*, 93–104.
Stammer, D., C. Wunsch, R. Giering, C. Eckert, P. Heimbach, J. Marotzke, A. Adcroft, C. N. Hill, and J. Marshall (2002), The global ocean circulation during 1992-1997, estimated from ocean observations and a general circulation model, *J. Geophys. Res.*, *107*(C9), 3118, doi:10.1029/2001JC000888.
Stommel, H. (1979), Determination of water mass properties of water pumped down from the Ekman layer to the geostrophic flow below, *Proc. Natl. Acad. Sci. U. S. A.*, *76*, 3051–3055.
Tandon, A., and K. Zahariev (2001), Quantifying the role of mixed layer entrainment for water mass transformation in the North Atlantic, *J. Phys. Oceanogr.*, *31*, 1120–1131.
Tziperman, E. (1986), On the role of interior mixing and air-sea fluxes in determining the stratification and circulation of the oceans, *J. Phys. Oceanogr.*, *16*, 680–693.
Tziperman, E., and W. C. Thacker (1989), An optimal-control/adjoint-equations approach to studying the oceanic general circulation, *J. Phys. Oceanogr.*, *19*, 1471–1485.
Valdivieso Da Costa, M., H. Mercier, and A. M. Treguier (2005), Effects of the mixed layer time variability on kinematic subduction rate diagnostics, *J. Phys. Oceanogr.*, *35*, 427–443.
Walin, G. (1982), On the relation between sea-surface heat flow and thermal circulation in the ocean, *Tellus*, *34*, 187–195.
Weller, R. A., P. W. Furey, M. A. Spall, and R. E. Davis (2004), The large-scale context for oceanic subduction in the northeast Atlantic, *Deep Sea Res., Part I*, *51*, 665–699.
Williams, R. G., J. Marshall, and G. Nurser (1995), Does Stommel's mixed layer "demon" work?, *J. Phys. Oceanogr.*, *25*, 3089–3102.
Woods, J. D. (1985), The physics of thermocline ventilation, in *Coupled Ocean–Atmosphere Models*, edited by J. C. J. Nihoul, pp. 543–590, Elsevier, New York.

G. Gebbie, Department of Earth and Planetary Sciences, Harvard University, 24 Oxford Street, Cambridge, MA 02138, USA. (gebbie@eps.harvard.edu)